

RESEARCH

Open Access



Thioredoxin: a key factor in cold tumor formation and a promising biomarker for immunotherapy resistance in NSCLC

Jiayi Hu^{1†}, Yilimunuer Abulimiti^{1†}, Haiyang Wang^{1†}, Dianyu Yang¹, Xu Wang¹, Yang Wang^{2*} and Ping Ji^{1*}

Abstract

Immune checkpoint blockade (ICB) therapy has shown promising clinical efficacy in cancer treatment, but only a subset of patients experience significant therapeutic responses. Tumor cells respond to internal and external stresses, such as hypoxia and nutrient deprivation, by activating the unfolded protein response (UPR) in the tumor microenvironment. This response helps maintain homeostasis, promoting malignant progression, chemotherapy resistance, and immune escape. In this study, single-cell RNA sequencing (scRNA-seq) data from non-small cell lung cancer (NSCLC) patients treated with ICB revealed upregulation of thioredoxin (TXN) expression in the epithelial tissues of LUAD (lung adenocarcinoma) and LUSC (lung squamous cell carcinoma) patients with minimal pathological remission. High TXN expression was also associated with “cold tumors,” characterized by a lack of T cells and low levels of chemokine receptors and immunomodulators. Experimental results showed that TXN was highly expressed in NSCLC tissues, and its knockdown significantly inhibited the proliferation and migration of A549 and SK-MES-1 cells. Furthermore, TXN knockdown enhanced T-cell-mediated cytotoxicity against these tumor cells, suggesting that TXN contributes to immune escape in NSCLC by promoting tumor cell proliferation and migration while inhibiting immune killing. Notably, TXN knockdown also upregulated CD40 expression, indicating that TXN may regulate immune escape in lung cancer through CD40 modulation.

Keywords NSCLC, Immune checkpoint Blockade (ICB) therapy, Thioredoxin (TXN)

Introduction

Lung cancer, particularly non-small cell lung cancer (NSCLC), is one of the deadliest malignancies worldwide, accounting for approximately 85% of all cases [1]. Due to its frequent diagnosis at advanced stages and the presence of metastases at diagnosis, treatment efficacy is limited, resulting in poor patient survival rates. In recent years, immune checkpoint blockade (ICB) therapy, particularly targeting the PD-1/PD-L1 pathway, has emerged as a breakthrough in NSCLC treatment. Studies have demonstrated that combination immunotherapy with PD-1/PD-L1 antibodies improves progression-free survival (PFS) and overall survival (OS) in NSCLC patients [2–4]. However, the objective response rate of PD-1/

[†]Jiayi Hu, Yilimunuer Abulimiti and Haiyang Wang contributed equally to this work.

*Correspondence:

Yang Wang
13639908783@139.com

Ping Ji
ji-ping1231@tongji.edu.cn

¹Department of Laboratory Medicine, Shanghai Tongji Hospital, School of Medicine, Tongji University, Shanghai 200065, China

²Department of Laboratory Medicine, Second Affiliated Hospital of Xinjiang Medical University, Xinjiang 830063, PR China



PD-L1 inhibitors remains relatively low, at approximately 20-40%, with only around 50% response in patients exhibiting high PD-L1 expression. Moreover, anti-PD-1 therapy benefits only a subset of patients, many of whom develop resistance over time [5, 6].

Several strategies have been identified to potentially enhance the therapeutic efficacy of immune checkpoint inhibitors (ICIs) in cancer treatment. These include: enhancing tumor cell immunogenicity [7]; targeting oncogenes to inhibit tumor cell growth and reduce their immune escape capabilities [8]; promoting T cell infiltration and activation within tumor tissues to enhance the cytotoxic effects on tumor cells [9]; reshaping the immunosuppressive tumor microenvironment by modulating cytokines, chemokines, and other relevant molecules [10]; targeting alternative immune checkpoints and immune-stimulatory receptors; and combining immunotherapy with other therapeutic modalities, such as surgery, radiotherapy, and chemotherapy, to maximize therapeutic outcomes and improve patient survival rates. Importantly, all these strategies face a critical challenge: overcoming immune escape driven by the endogenous factors of tumor cells. Therefore, understanding the mechanisms by which tumor cells intrinsically inhibit ICI efficacy is essential for improving therapeutic responses.

In tumor therapy, drug-induced cell death, abnormal transcription, and metabolic changes significantly increase the burden on protein synthesis within cells. The endoplasmic reticulum (ER), as the primary site of protein synthesis, folding, and processing, must adapt to these changes to maintain cellular stability [11, 12]. However, as tumor cells proliferate and encounter stress, misfolded proteins accumulate in the ER, triggering the unfolded protein response (UPR) to restore homeostasis [13]. Generally, UPR alleviates ER burden and damage, restores protein synthesis, and maintains ER function. However, prolonged or excessive UPR activation can impair ER function, leading to a condition known as ER stress, which may contribute to increased resistance to treatment, particularly during immunotherapy and chemotherapy [14, 15]. Recent studies have highlighted targeting ER stress as a promising anti-tumor strategy with broad therapeutic potential [15, 16].

In this study, we analyzed scRNA-seq data from NSCLC patients treated with PD-1/PD-L1 antibodies and found that Thioredoxin (TXN) was upregulated in lung epithelial cells in both lung adenocarcinoma (LUAD) and lung squamous cell carcinoma (LUSC) patients, with no major pathological changes observed. The TXN system plays a crucial role in the removal of reactive oxygen species (ROS), and its inhibition leads to elevated ROS levels, oxidative damage, and cell death. Some enzymes of the TXN system exert anti-apoptotic effects through direct interactions with key signaling proteins. For example,

TXN1 interacts with apoptosis signal-regulating kinase 1 (ASK1) to prevent its pro-apoptotic signaling. PRDX functions as a chaperone for several oncogenes and tumor suppressors, such as mitogen-activated protein kinases (MAPK) [17], c-MYC [18], and phosphatase and tensin homolog (PTEN) [19]. Studies have shown that in chronic lymphocytic leukemia cells, AUR kinase triggers ER stress and induces apoptosis [20]. ER stress is induced by the accumulation of misfolded or damaged proteins, which activates the UPR pathway to alleviate the stress; however, persistent, unresolved ER stress ultimately leads to cell apoptosis. Inhibition of TXNRD1 disrupts disulfide bond folding in the ER, establishing a direct link between cytoplasmic oxidative stress and ER stress [21]. While the role of TXN in redox processes has been extensively studied, its influence on the effectiveness of immunotherapy remains underexplored. In this study, we further investigated the expression and immune-related effects of TXN in NSCLC and found that high TXN expression was associated with the formation of “cold tumors,” characterized by T cell deficiency and low expression of chemokine receptors and immune modulatory molecules. Targeting TXN could potentially enhance the effectiveness of ICB therapy in NSCLC.

Materials and methods

Analysis of NSCLC ICB therapy scRNA-Seq data

The NSCLC scRNA-Seq ICB therapy dataset was sourced from GSE207422 in the GEO database [22]. This scRNA-Seq dataset originates from the surgically resected tissues of 12 patients with NSCLC after treatment. All these patients were found to have no EGFR/ALK mutations. These patients received neoadjuvant therapy, which included 2 to 4 cycles (each cycle lasting 3 weeks) of PD-1 antibody combined with platinum-based chemotherapy. After the treatment, the samples were classified into two groups based on the pathological assessment: major pathological response (MPR, $n = 4$) and non-major pathological response (NMPR, $n = 8$).

Analysis was performed using the Seurat package in R [23–25], generating a unique molecular identifier (UMI) matrix for each sample. During quality control (QC), cells were excluded based on the following criteria: fewer than 500 expressed genes, more than 20% UMI from mitochondrial genes, more than 50% UMI from ribosomal genes, or a housekeeping gene score < 1 (ACTB, GAPDH, MALAT1). Doublets were detected and removed using Scrublet (version 0.2.1) with an expected doublet rate of 0.025 and a manually selected threshold. The gene expression matrix was normalized using the NormalizeData function, and cross-sample variation was adjusted using Seurat’s anchor-based integration workflow. The integrated data was used for dimensionality reduction and clustering, visualized via

PCA and UMAP. Cell clusters were assigned to specific lineages based on marker gene abundance, with markers identified using the FindAllMarkers function. Epithelial cells were extracted for downstream analysis. Differential expression analysis was performed using the FindAllMarkers function, comparing gene expression between groups. Pathway enrichment analysis was conducted with the GSVA package (version 1.38.2) based on scRNA-seq data [26].

Evaluation of immunological characteristics of the TME in TCGA-LUAD and TCGA-LUSC

mRNA expression and TMB data for TCGA-LUAD and TCGA-LUSC were retrieved from the UCSC Xena platform (<https://xena.ucsc.edu/>). Differences in immune cell infiltration were evaluated using single-sample gene set enrichment analysis (ssGSEA) with the “GSVA” package. The ESTIMATE algorithm was used to calculate stromal, immune, and ESTIMATE scores for each sample based on ssGSEA. Cancer-immunity cycle scores for TCGA-LUAD and TCGA-LUSC were obtained from the TIP database (<http://biocc.hrbmu.edu.cn/TIP/>). We collected data from published articles on immunomodulators, including damage-associated molecular patterns, MHC molecules, receptors, chemokines, immunostimulants, and inhibitory immune checkpoints with therapeutic potential. To investigate the role of TXN in regulating the immune characteristics of the tumor microenvironment in TCGA-LUAD and TCGA-LUSC, we performed Pearson correlation analysis to examine the correlation between TXN expression and the immune-related gene sets mentioned above.

Verification of the role of TXN at the single-cell level in regulating the immune microenvironment of NSCLC

The dataset used to validate TXN expression and TME immunological characteristics was derived from the study by Philip et al. [27]. Data quality control was conducted using the same methods and parameters as those used for the previously mentioned scRNA-Seq ICI dataset. The cutoff value for TXN expression was determined based on the average expression level of TXN in each tumor sample, with patients classified into high-expression and low-expression groups accordingly.

Cell-cell communication potential was assessed using the CellChat R package (version 1.1.3) [28]. The normalized expression matrix was imported to create a CellChat object using CellChat functions. Preprocessing was performed using the identify Over Expressed Genes, identify Over Expressed Interaction, and Project Data functions with default parameters. Potential ligand-receptor interactions were identified through the compute Commun-Prob, filter Communication, and compute Commun Prob Pathway functions. Finally, the aggregate Net function

was employed to aggregate the cell communication network. Major signaling sources and targets were identified by evaluating the outgoing and incoming interaction strengths as out-degree and in-degree centrality metrics within the weighted cell communication network, with edge weights determined by the communication probabilities computed by CellChat.

Differentially expressed genes between clusters or groups in the scRNA-seq data were explored using the FindMarkers function. For scRNA-seq gene set analysis, pre-ranked gene set enrichment analysis (GSEA) was conducted using the ‘fgsea’ R package, or gene set variation analysis (GSVA) was performed using the ‘gsva’ R package.

Cell lines and cultures

The human NSCLC cell lines A549 and SK-MES-1 were purchased from the Cell Bank of the Chinese Academy of Sciences (Shanghai, China). The cells were cultured in high-glucose Dulbecco’s Modified Eagle’s Medium (DMEM, Gibco), supplemented with GlutaMAX, 10% fetal bovine serum (FBS, Hyclone), and 100 U/mL penicillin-streptomycin (Invitrogen). The interfering sequences of the human TXN gene were selected to design shRNA fragments (5'-AAAGGACGCUGCAGGUGAUAATTTAGTGAGGAGGACGCUGCAGGUGAUAATTTTT-3'). The empty vector and shRNA were transfected into A549 and SK-MES-1 cells using pLent-U6-GFP-Puro as the vector, and then cultured with the ADV-HR viral helper factor to observe the efficiency of green fluorescence and verify the knockdown effect. Stable transfected cell lines with knockdown of the human TXN gene were constructed by screening with puromycin.

T cell activation and expansion

Purified T cells should be activated at an optimal surface density of 1×10^6 cells per cm^2 . Resuspend Purified T cells in 990 μL supplemented Medium with 20 IU/mL Human IL-2 or 155 U/mL Human IL-7 and 290 U/mL Human IL-15 in a 48-well plate. Add 10 μL of the T Cell TransAct (Miltenyi Biotec, 130-128-758), then incubate at 37 °C, 5% CO_2 for up to 3 days. When working with higher cell numbers, scale up all reagent volumes and total volumes accordingly.

RNA extraction and real-time quantitative PCR analysis

Cells or tissues were lysed using TRIzol reagent (Invitrogen, USA) to extract total RNA. The RNA concentration was measured using a NanoDrop 2000 spectrophotometer (Thermo, USA) at 260 nm. RNA was reverse transcribed into cDNA using the PrimeScript RT reagent (TaKaRa, Japan), according to the manufacturer’s instructions. The resulting cDNA was stored at -20 °C for further

use. TXN mRNA expression was quantified using quantitative real-time PCR (qRT-PCR) on an ABI 7500 system (Thermo, USA). SYBR Premix (TaKaRa, Japan) was used for qRT-PCR, following the manufacturer's instructions. Amplification and melting curves were analyzed to confirm the specificity of the amplification, and GAPDH and β -actin were used as reference genes. The CT values of the target gene were obtained, and relative gene expression in each experimental group was calculated using the $\Delta\Delta$ CT method. TXN primers were synthesized by Shanghai Sangon Biotech Co., Ltd. (China), with the forward primer sequence being GTGAAGCAGATCGAGA GCAAG and the reverse primer sequence being CGTGG CTGAGAAGTCAACTACTA.

Western blot analysis of TXN expression

Western blot (WB) was used to detect the expression of TXN in tissues or cells. To extract total protein, cells were lysed in RIPA buffer containing protease inhibitors (Beyotime, P1005, 1:100). The total protein samples were loaded onto Bis-Tris SDS/PAGE gels and then transferred to polyvinylidene fluoride (PVDF) membranes. The membranes were blocked with 5% BSA for 1 h, followed by incubation with anti-TXN antibody (Thioredoxin 1, CSTC63C6, 1:1000) at 4 °C overnight. The membranes were then incubated with the secondary antibody (Beyotime, P0208, 1:1000) for 1 h. Finally, bands were detected using the DAB kit and analyzed with an imaging system.

CCK-8 assay and colony formation assay

The CCK-8 assay was performed according to the manufacturer's instructions (Beyotime, C0038). Cell proliferation was quantified by measuring the optical density at 450 nm (OD450). For the colony formation assay, 1000 cells were seeded into each well of a six-well plate and cultured in a 37 °C incubator with 5% CO₂. After the incubation period, the cells were washed with phosphate-buffered saline (PBS), fixed with methanol, and stained with crystal violet. The colonies were then visualized and counted under an optical microscope.

Scratch assay for cell migration

A549 and SK-MES-1 cells were seeded into 6-well plates at a density of 1×10^5 cells/ml in 2 mL of cell suspension. Each group was performed in triplicate. To create the scratch, vertical lines were made on the cell monolayer using sterile pipette tips. After scratching, the cells were washed twice with PBS to remove debris and incubated in serum-free medium. Migration of cells into the scratched area was observed at 0, 24, and 48 h using an inverted microscope. The width of the wound was measured at five randomly selected fields ($\times 100$ magnification) per group, and the percentage of wound closure was calculated.

Flow cytometry

A549 and SK-MES-1 cells were seeded at a density of 1×10^5 cells per well in 60 mm culture plates and cultured in RPMI-1640 medium supplemented with 10% fetal bovine serum (FBS) at 37 °C in a humidified incubator with 5% CO₂ for 24 h. After 24 h, cells were treated with 5 μ M decitabine (HY-A0004, MedChemExpress, New Jersey, USA) dissolved in DMSO for 24 h, with the control group receiving an equal volume of DMSO. Cells were harvested using 0.25% trypsin-EDTA (Gibco, Thermo Fisher), incubated at 37 °C for 3-5 min, and then gently detached. The reaction was stopped by adding complete culture medium containing 10% FBS. Cells were collected by centrifugation at $300 \times g$ for 5 min and washed twice with cold PBS. For immunostaining, cells were blocked with 5% BSA in PBS for 30 min at 4 °C, followed by incubation with FITC Mouse Anti-Human CD40 antibody (Cat. No. 556624, BD Biosciences) at a dilution of 1:100 for 30 min at 4 °C. Flow cytometry analysis was performed using a Cytex Aurora flow cytometer (Cytex Biosciences). FITC fluorescence was detected in the FL1 channel, and at least 10,000 events per sample were collected. Data analysis was performed using FlowJo software (FlowJo, LLC).

Quantification and statistical analysis

All statistical analyses described above were performed either with R or with Prism 10 (GraphPad Software). The following statistical significance levels were used: * $p < 0.05$, ** $p < 0.01$, *** $p < 0.001$, and **** $p < 0.0001$.

Results

High TXN expression in epithelial cells correlates with PD-1 antibody resistance in NMPR NSCLC

This study focused on epithelial cell-driven PD-1 antibody resistance in combination with chemotherapy. We analyzed published single-cell sequencing data from 12 surgically resected patients receiving PD-1 antibody combined with chemotherapy, including 4 patients with MPR and 8 patients with NMPR [22]. After quality assurance and filtering of individual cells, a total of 74,091 high-quality cells were obtained from the GSE207422 dataset, including 23,171 cells from MPR patient tissue and 55,171 cells from NMPR patient tissue. After removing unwanted cells, the data were combined. Based on the expression of classical marker genes [29], we annotated the cell clusters as different types of immune and non-immune cells, including T cells, NK cells, B cells, myeloid cells, neutrophils, plasma cells, plasmacytoid dendritic cells (pDC), mast cells, stromal cells (fibroblasts/endothelial cells), and epithelial cells. Epithelial cells were extracted, regrouped, and divided into nine subpopulations (Fig. 1A).

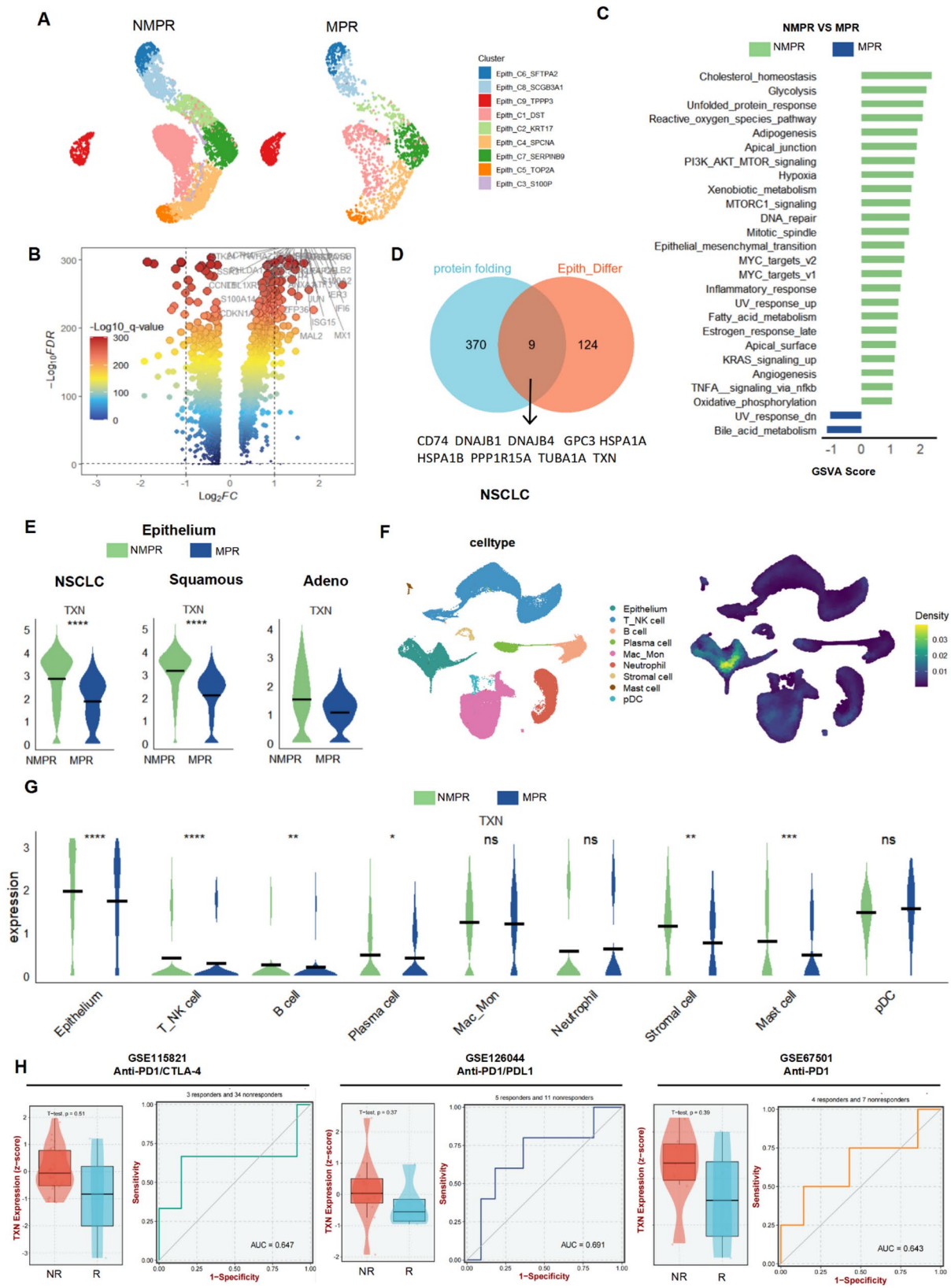


Fig. 1 (See legend on next page.)

(See figure on previous page.)

Fig. 1 High TXN Expression in Epithelial Cells Correlates with PD-1 Antibody Resistance in NMPR NSCLC. **(A)** UMAP visualization of epithelial cells from MPR and NMPR patients based on scRNA-seq data from the GSE207422 dataset. **(B)** Volcano plot showing differentially expressed genes in epithelial cells from MPR and NMPR patients. **(C)** GSEA of differentially expressed pathways in these epithelial cells. **(D)** Venn diagram illustrating the overlap of differentially expressed UPR-related genes in MPR and NMPR patients. **(E)** TXN expression in epithelial cells from NSCLC, including LUAD and LUSC subtypes, in MPR and NMPR patients. **(F)** UMAP visualization of TXN expression across various cell types from MPR and NMPR patients based on scRNA-seq data. **(G)** Violin plot showing TXN expression in different cell types from MPR and NMPR NSCLC patients. **(H)** TXN expression in patients with non-response (NR) and response (R) to ICB treatment (left), and the diagnostic ROC curve for predicting treatment response (right)

Differential gene expression and GSEA revealed that major pathways up-regulated in NMPR included cholesterol homeostasis, glycolysis, unfolded protein response, reactive oxygen species pathway, adipogenesis, and others (Fig. 1B-C). The UPR caught our attention. Both chemotherapy and radiotherapy trigger mechanisms such as DNA damage and oxidative stress, causing cancer cells to react to stress, which leads to the accumulation of large amounts of unfolded proteins. Endoplasmic reticulum stress attempts to restore homeostasis by initiating the UPR, pathways through which tumor cells regulate not only protein folding and modification but also their metabolic pathways and immune escape mechanisms, thereby helping tumor cells survive and proliferate in an adverse therapeutic environment.

Through the intersection analysis of differential genes with published UPR-related gene sets, we identified nine differentially expressed UPR genes in MPR and NMPR groups (Fig. 1D and Table S1). Further analysis revealed that these nine genes exhibited significant expression heterogeneity across different tissue types. In LUAD ($n=6$) and LUSC ($n=6$), only the differential expression of TXN and CD74 showed a consistent trend. TXN was upregulated in both LUAD and LUSC (Fig. 1E and Supplementary Fig. 1A), while CD74 was downregulated in both cancer types (Supplementary Fig. 1B). Further investigation showed that TXN was primarily highly expressed in epithelial cells (Fig. 1F-G), whereas CD74 was predominantly expressed in B cells. Additionally, in the Biomarker Exploration of Solid Tumors (BEST) database^[54], TXN expression was consistently higher in patients who did not respond to ICB treatment in the GSE115821, GSE126044, and GSE67501. This study focused on the mechanism of PD-1 antibody resistance driven by epithelial cells, particularly in combination with chemotherapy. Therefore, TXN, which is predominantly expressed in epithelial cells, was selected for further investigation.

TXN is associated with a non-inflammatory tumor immune microenvironment in NSCLC

The infiltration of immune cells and their ability to recognize tumor-specific antigens are crucial indicators of the efficacy of immune checkpoint inhibitors. To explore the role of TXN in the tumor immune response, we analyzed the correlation between TXN expression and immune cell infiltration using the single-sample gene set enrichment analysis (ssGSEA) algorithm, based on the

TCGA-LUAD and TCGA-LUSC datasets. The results indicated that tumors with high TXN expression exhibited significantly lower levels of CD8⁺ T cells, NK cells, Th1 cells, macrophages, and dendritic cells compared to those with low TXN expression (Fig. 2A, Supplementary Fig. 2A-B, and Table S2). This suggests that high TXN expression is associated with the formation of “cold tumors,” characterized by a lack of T cell infiltration. Further analysis of the tumor microenvironment (TME) showed that, in the high TXN expression group, matrix, immune, and estimated scores were significantly reduced (Fig. 2B and Table S3). To investigate the relationship between TXN and the immune response, we used the Tumor Immunophenotype Tracking (TIP) analysis platform [30] to examine TXN expression across various stages of the cancer immune cycle. In both LUAD and LUSC, high TXN expression was associated with downregulated activity in key steps of the immune cycle, including tumor antigen presentation (step 2), immune cell activation (step 3), immune cell migration to the tumor (step 4), immune cell invasion (step 5), T cell recognition of cancer cells (step 6), and cancer cell killing (step 7) (Fig. 2C and Table S4).

While high TMB is often correlated with the expression of neoantigens that activate the immune response [31], we observed a weak correlation between TMB and TXN expression in high-TXN tumors in both LUAD and LUSC (Fig. 2D and Table S5), suggesting that TXN may not strongly induce neoantigen responses through mutations. Immune checkpoint blockers rely on adaptive anti-tumor immune responses activated by a combination of tumor antigens and DAMPs molecules. Correlation analysis revealed that TXN expression was negatively correlated with most DAMPs, including TLR2, TLR4, TLR7, NLRP3, BCL2, IL33, CLEC7A, FPR1, FPR2, and AGER, but positively correlated with HMGB1, PPIA, and HSP90 (Fig. 2E and Table S6). In both TCGA-LUAD and TCGA-LUSC, there was significant heterogeneity in the correlation between TXN and chemokines (Table S7). However, chemokine receptors such as CCR1, CCR2, CCR4, CCR5, CCR7, CCR8, CCR9, XCR1, CXCR2, CXCR4, CXCR5, CXCR6, and IL2RA were generally negatively correlated with TXN expression (Table S8). These receptors are involved in the recruitment of CD8⁺ T cells, Th17 cells, and antigen-presenting cells, suggesting that TXN may inhibit excessive immune cell recruitment and inflammatory responses via negative regulatory mechanisms.

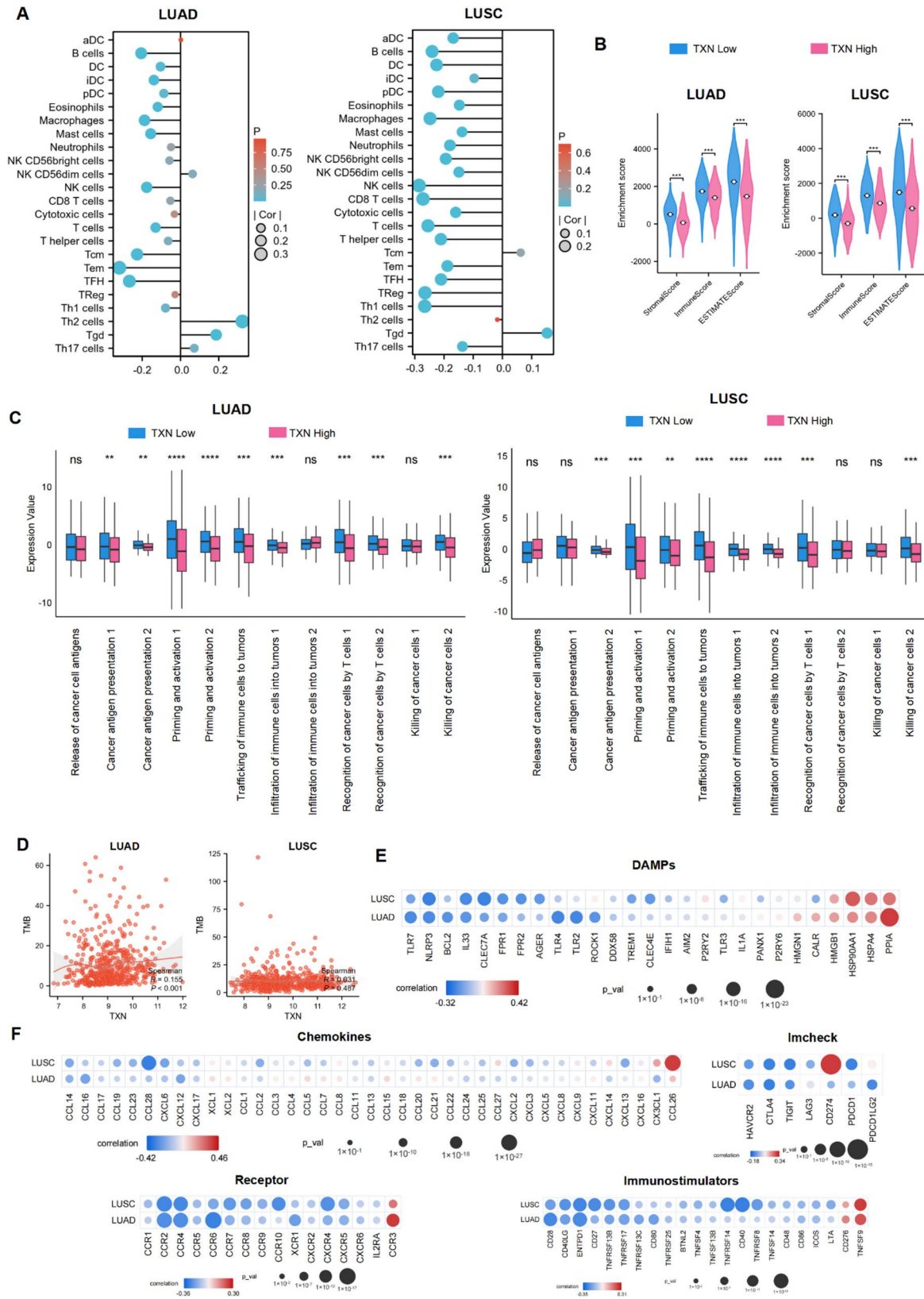


Fig. 2 (See legend on next page.)

(See figure on previous page.)

Fig. 2 TXN is associated with a non-inflammatory tumor immune microenvironment in NSCLC. **(A)** Correlation between TXN expression and immune cell infiltration in TCGA-LUAD and TCGA-LUSC, assessed by ssGSEA. **(B)** Comparison of StromaScore, ImmuneScore, and ESTIMATE scores between TXN-High and TXN-Low subgroups, showing lower scores in the TXN-High group. **(C)** Comparison of cancer immune cycle activity between TXN-High and TXN-Low subgroups in TCGA-LUAD and TCGA-LUSC. **(D)** Correlation between TXN expression and tumor mutation burden (TMB) in TCGA-LUAD and TCGA-LUSC. **(E)** Correlation between TXN expression and damage-associated molecular patterns (DAMPs) in TCGA-LUAD and TCGA-LUSC. **(F)** Correlation between TXN expression and chemokines, receptors, and immunostimulatory molecules in TCGA-LUAD and TCGA-LUSC

Additionally, TXN was inversely associated with several immunostimulatory molecules, including CD28, CD40LG, ENTPD1, CD27, CD40, CD80, and TNFRSF family members, which are crucial for T cell activation (Table S9). Notably, PDL1 (CD274) was positively correlated with TXN expression in LUSC, while most inhibitory immune checkpoints were significantly down-regulated in high TXN expression tumors (Fig. 2F and Table S10). In the GSE207422 scRNA-Seq dataset of ICB patients, we observed that CD274 expression in epithelial cells was significantly higher in MPR patients compared to NMPR patients. However, no significant correlation was found between TXN expression in epithelial cells and CD274. Interestingly, increased TXN expression in epithelial cells was associated with higher average expression levels of immune inhibitory receptors on T-cell subsets, including TPDCD1, HAVCR2 (TIM3), CTLA4, and LAG3 (Supplementary Fig. 3). These findings suggest that high TXN expression in NSCLC may be associated with impaired immune cell infiltration, suppressed immune responses, and inhibition of T cell activation.

High TXN expression disrupts NSCLC immune surveillance

We further investigated the relationship between TXN expression and the NSCLC tumor microenvironment at the single-cell level using the other NSCLC dataset [27]. A subset analysis of 34,708 high-quality cells was performed, with cell clusters categorized into immune and non-immune cells based on classical marker gene expression (Fig. 3A). Samples with TXN levels greater than 1 were classified as the “TXN-high” group, while samples with TXN levels less than 1 were classified as the “TXN-low” group (Fig. 3B-C). Consistent with the TCGA database, the proportion of T and NK cells in the “TXN-high” group was significantly lower than in the “TXN-low” group (Fig. 3D). Next, cell interactions between the “TXN-high” and “TXN-low” groups were quantified using CellChat, with interaction frequency indicated by line thickness. The total number of interactions was lower in the “TXN-high” group, although the interaction intensity was higher compared to the “TXN-low” group (Supplementary Fig. 4A-B).

In the “TXN-high” group, signaling pathway intensity from tumor cells to myeloid cells, endothelial cells, and fibroblasts was significantly higher than in the “TXN-low” group (Fig. 3E). Network centrality analysis revealed that myeloid cells were the primary contributors to cell

communication in the “TXN-high” group, whereas T and NK cells dominated the “TXN-low” group (Fig. 3F). Additionally, CADM, a marker associated with host immune surveillance, and co-stimulatory receptor CD226 signaling in tumor epithelial cells were elevated in the “TXN-high” group compared to the “TXN-low” group (Fig. 3G and Supplementary Fig. 4C-F). Differential expression analysis of the UPR pathways between the “TXN-high” and “TXN-low” groups revealed that tumor cells in the “TXN-high” group exhibited upregulated pathways, similar to those in the NMPR group. These pathways included UPR, ROS pathways, and DNA repair mechanisms, as shown in Fig. 3H-I.

TXN facilitates proliferation and migration while inhibiting Immune-Mediated killing in NSCLC

To investigate the expression and functional role of TXN in NSCLC, we first analyzed data from the TCGA database. The results indicated that the mRNA level of TXN was significantly higher in LUAD and LUSC tissues compared to paired normal tissues (Fig. 4A). We then confirmed this finding by qPCR analysis of TXN mRNA expression in 20 LUAD and LUSC samples, which showed significantly higher expression in both cancer types than in matched non-tumor tissues (Fig. 4B). Western blotting further confirmed that TXN protein expression was significantly elevated in LUAD and LUSC cancerous tissues compared to matched non-tumor tissues (Fig. 4C).

To explore the role of TXN in cell proliferation, TXN expression was knocked down in A549 (lung adenocarcinoma) and SK-MES-1 (lung squamous cell carcinoma) cells. Cell proliferation was then assessed using CCK-8 and colony formation assays. The results showed that TXN knockdown significantly inhibited proliferation and colony formation in both A549 and SK-MES-1 cells (Fig. 4D, E). Migration assays revealed that TXN knockdown also significantly reduced the migration ability of both cell lines (Fig. 4F). Finally, we assessed the role of TXN in immune escape by establishing a co-culture model of Jurkat T cells with A549 or SK-MES-1 cells, which were stimulated and activated with CD3/CD28 T cell transAct. The results showed that TXN knockdown significantly enhanced the immune killing effect of T cells on both A549 and SK-MES-1 cells (Fig. 4G). These findings suggest that TXN may play a critical role in tumor

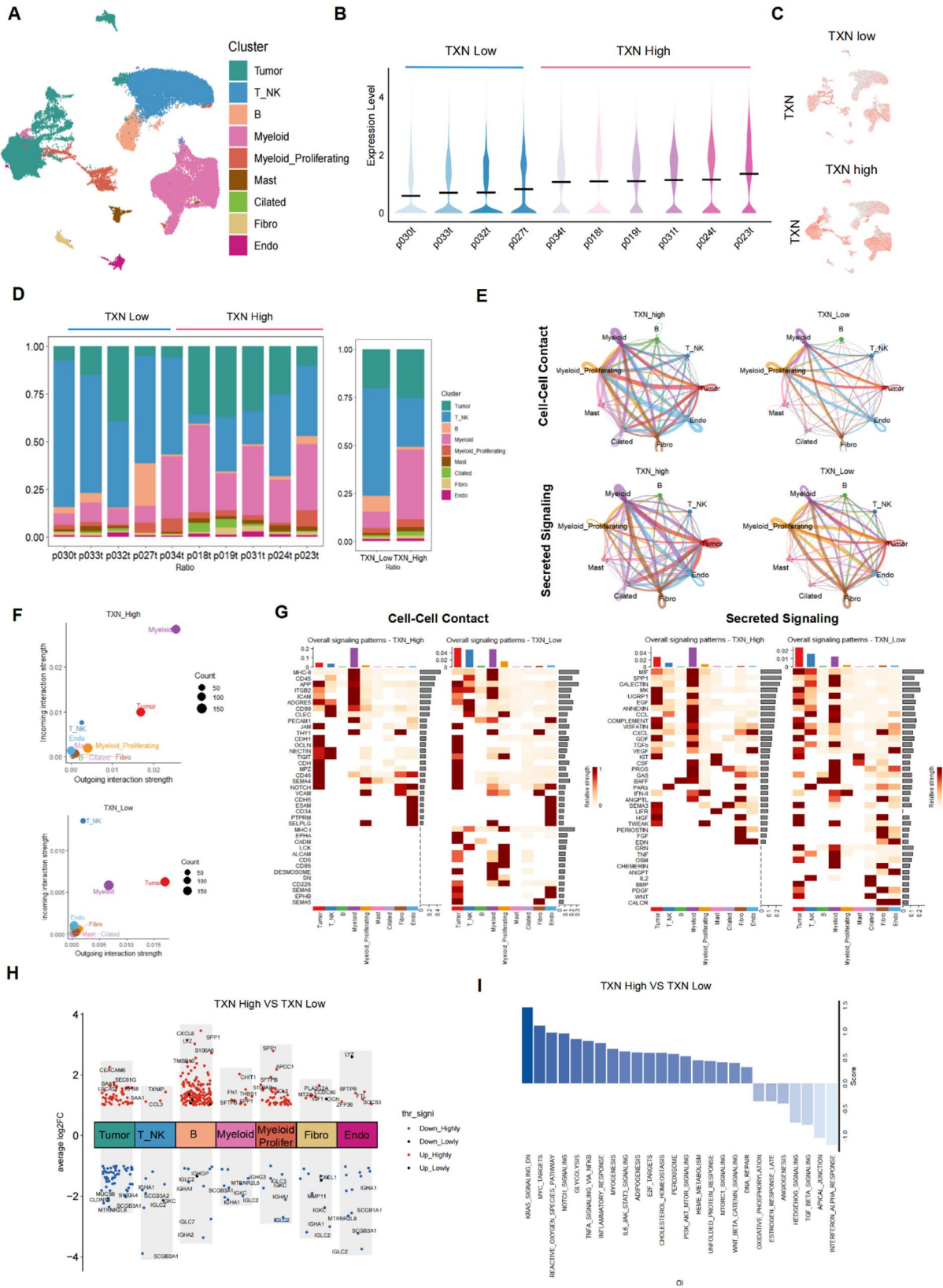


Fig. 3 (See legend on next page.)

(See figure on previous page.)

Fig. 3 High TXN expression disrupts NSCLC immune surveillance. All data were based on scRNA-seq data from the study by Philip et al. [27]. **(A)** UMAP visualization of the scRNA-seq data. **(B)** Classification of samples into “TXN-high” and “TXN-low” groups based on TXN expression levels. **(C)** UMAP visualization of TXN expression in the “TXN-high” and “TXN-low” groups. **(D)** Relative proportion of immune cell subsets in the “TXN-high” and “TXN-low” groups. **(E)** CellChat analysis of signaling pathway intensity between the “TXN-high” and “TXN-low” groups. **(F)** Network centrality analysis of cell communication in the “TXN-high” and “TXN-low” groups. **(G)** Heatmap of overall cell-cell contact and secreted signaling communication intensity in the “TXN-high” and “TXN-low” groups. **(H)** Volcano plot showing differentially expressed genes between the “TXN-high” and “TXN-low” groups across various cell subpopulations. **(I)** GSVA analysis of differentially expressed pathways in the “TXN-high” and “TXN-low” groups

immune escape in NSCLC by promoting cell proliferation, migration, and inhibiting immune killing.

TXN down-regulates CD40 expression in NSCLC cells

To further investigate the potential mechanism of TXN in cell proliferation and the formation of low immune cell infiltration in NSCLC, we screened genes positively correlated (Pearson > 0.3) and negatively correlated (Pearson < 0.3) with TXN expression from the TCGA-LUAD and TCGA-LUSC databases, respectively (Fig. 5A Table S11). In these two datasets, TXN expression was positively correlated with 469 genes and negatively correlated with 140 genes. Gene Ontology (GO) analysis of these differentially expressed genes revealed enrichment in several biological processes (GO-BP), including protein synthesis and folding (e.g., ribonucleoprotein complex biosynthesis, protein folding, protein stability regulation), energy metabolism (e.g., energy harvesting from oxidation of organic compounds, ATP metabolic processes), RNA processing and post-transcriptional regulation (e.g., mRNA processing, RNA splicing, RNA localization), and nucleotide metabolism (e.g., nucleotide metabolic processes, nucleotide biosynthesis) (Fig. 5B and Table S12).

To predict the interaction between TXN and related genes, we used the GeneMANIA website (<http://genemania.org/>), which identified a significant regulatory relationship between TXN and CD40 (Fig. 5C and Table S13). To further explore this interaction, we utilized AlphaFold3 to predict a hydrogen bond between the 72nd Lysine (Lys72) of TXN and the 59th Cysteine (Cys59) of CD40, suggesting a potential molecular interaction. CD40, a 48 kDa transmembrane glycoprotein in the tumor necrosis factor receptor (TNFR) superfamily, is expressed in various cell types, including antigen-presenting cells (e.g., dendritic cells, macrophages, B cells) and certain tumor cells [32, 33]. Importantly, CD40 is upregulated in cancer cells but not in normal cells, where it plays a crucial role in promoting apoptosis and/or necrosis signaling, contributing to tumor cell death. CD40 expression in lung cancer is strongly associated with immune escape and tumor progression [34]. We observed a negative correlation between TXN expression and CD40, as well as CD40L expression, in both TCGA-LUAD and TCGA-LUSC datasets. To verify this, we examined the effect of TXN knockdown on CD40 expression in A549 and SK-MES-1 cells using flow cytometry. Given the low basal expression of CD40 in these NSCLC

cell lines, we treated cells with 5 μ M decitabine to induce CD40 expression [35]. The results demonstrated that TXN knockdown significantly upregulated CD40 expression in both cell lines, indicating that TXN may contribute to immune escape in NSCLC by modulating CD40 expression.

Discussion

ICB therapy has shown promising clinical outcomes in cancer treatment; however, only a subset of patients exhibit significant responses to this approach. Tumor cells respond to both internal and external stresses, including hypoxia and nutrient deficiency, by activating an UPR in the tumor microenvironment. This adaptive mechanism enables cancer cells to maintain homeostasis and promotes malignant progression, chemotherapy resistance, and immune evasion [36, 37].

UPR plays a critical role in tumor cell survival under adverse microenvironmental conditions by regulating protein folding and repair processes, especially during stress such as oxygen and nutrient deprivation. This activation of UPR enhances protein folding and alleviates ER stress, which helps tumor cells adapt to harsh conditions. Different branches of the UPR regulate tumor cell growth, survival, and immune response, potentially influencing the efficacy of ICB therapy by modulating the tumor immune landscape [38]. Studies suggest that tumor cells also activate the UPR to escape the effects of immune checkpoint inhibitors through immune evasion mechanisms [39, 40]. These findings highlight the potential of targeting the UPR signaling pathway to improve clinical immunotherapy outcomes.

In this study, scRNA-seq data from NSCLC patients treated with ICB showed that TXN expression was upregulated in the epithelial tissues of LUAD and LUSC patients with a non-major pathologic response. TXN, which encodes the REDOX enzyme Trx1, plays a crucial role in maintaining REDOX homeostasis, regulating free radicals and reactive oxygen species to counteract oxidative stress [41, 42]. TXN also contributes to cell proliferation, immune evasion, and inflammation. Its knockdown inhibits tumor cell growth, suggesting its catalytic role in these processes [43]. The TXN system, including key enzymes like TXN, TXNRD, and PRDX, is essential for protein folding and preventing misfolding in the ER [44]. Inhibition of this system disrupts disulfide bond formation, leading to unfolded protein accumulation, UPR

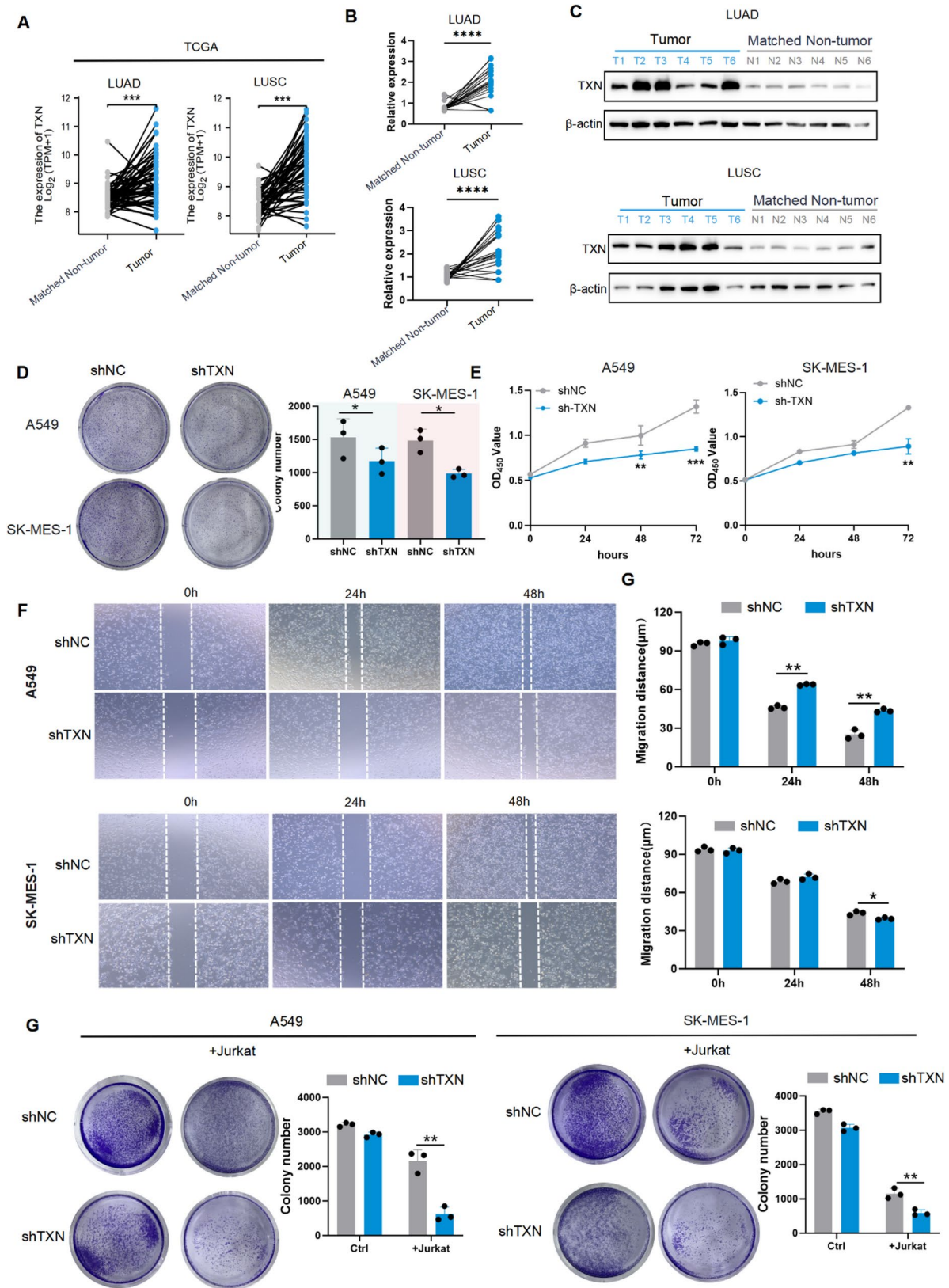


Fig. 4 (See legend on next page.)

(See figure on previous page.)

Fig. 4 TXN Facilitates Proliferation and Migration while Inhibiting Immune-Mediated Killing in NSCLC. **(A)** TXN mRNA expression in TCGA-LUAD and TCGA-LUSC tumor and matched non-tumor tissues. **(B)** RT-qPCR analysis of TXN mRNA expression in 20 LUAD and LUSC tumor and matched non-tumor tissues. **(C)** Western blot analysis of TXN protein expression in LUAD and LUSC tumors and matched-non tissues. **(D-E)** Colony formation and CCK-8 assays assessing the impact of stable TXN knockdown on A549 and SK-MES-1 cell survival and proliferation ($n=3$). **(F)** Cell migration assay showing the effect of stable TXN knockdown on A549 and SK-MES-1 migration. **(G)** Survival of tumor cells co-cultured with activated Jurkat cells, assessed by crystal violet staining

activation, and potential apoptosis if the stress is unresolved [21, 45]. TXN and its encoded protein Trx1 have shown potential diagnostic and therapeutic value in various disease models. Elevated TXN expression has been observed during asthma attacks, in sepsis patients, and in patients with acute lung injury. Additionally, reduced TXN levels are associated with the severity of coronary artery disease [46]. Furthermore, inhibiting TXN may offer a promising strategy for cancer therapy [47].

We found that NSCLC patients with high TXN expression were more likely to develop “cold tumors,” characterized by T cell deficiency and low expression of chemokine receptors and immune modulators. The activity of the cancer immune cycle reflects the complex immunomodulatory interactions within the tumor microenvironment. Notably, both LUAD and LUSC patients with high TXN expression exhibited tumor antigen presentation, immune cell activation and migration to the tumor, and reduced T cell recognition and cancer cell killing. Tumor-specific antigens (neoantigens) are key inducers of T-cell-mediated immune responses, with their abundance commonly referred to as TMB [48]. Despite the negative correlation between high TXN expression and T cell-mediated cancer cell killing, the relationship between TMB and TXN expression was weak, suggesting that TXN may not directly drive a strong neoantigen response through mutations.

Chemokine receptors are crucial for leukocyte chemotaxis, immune cell recruitment, inflammatory response, and tumor progression. In both TCGA-LUAD and TCGA-LUSC datasets, we identified several chemokine receptors (e.g., CCR2, CCR5, CXCR4, CXCR7) that were negatively correlated with TXN expression. These receptors, particularly the CCR2/CCL2 and CCL5/CCR5 axes, drive lung cancer metastasis and poor prognosis [49]. Additionally, CXCR1 and CXCR2 are linked to drug resistance, while CXCR7 promotes tumor migration and metastasis in lung cancer [50–52]. These findings suggest that TXN may inhibit immune response and T cell activation in NSCLC by limiting immune cell infiltration. Interestingly, while PD-L1 (CD274) in LUSC was positively correlated with TXN expression, most other immune checkpoints were significantly downregulated in high TXN expression groups, potentially due to preexisting immune cell suppression in the tumor microenvironment. This implies that NSCLC patients with high TXN expression may have reduced sensitivity to ICBs.

Inadequate antigen presentation is a major mechanism of immune escape in NSCLC, where tumor cells inhibit immune recognition by impairing the ability of antigen-presenting cells (APCs), such as dendritic cells (DCs), to effectively capture, process, and display tumor antigens. This results in an impaired immune response initiation [53]. Furthermore, the lack of co-stimulatory molecules in the tumor microenvironment exacerbates immune evasion and accelerates tumor progression and metastasis. Our study reveals that high TXN expression correlates negatively with the expression of several DAMPs and immunostimulatory factors, including CD28, CD40, CD40LG, and CD80. CD28, a key co-stimulatory molecule, activates T cells by binding to CD80 or CD86 [54–56]. CD40 and its ligand CD40L (CD154), primarily expressed by activated T cells, play a critical role in antigen cross-presentation to DCs and T cell activation [57, 58]. Recent studies have highlighted that CD40 is widely expressed in various tumors, including lung cancer, and its expression enhances tumor immune responses. Transduction of DCs and tumor cells with the CD40L gene has shown persistent immune responses in preclinical models [59]. Based on this, we hypothesize that TXN may contribute to immune escape in NSCLC by downregulating CD40 expression, thereby inhibiting effective antigen presentation and T cell activation.

Overall, our findings suggest that elevated TXN expression in NSCLC patients correlates with poor responses to immunotherapy. Patients with high TXN levels are more likely to exhibit “cold tumors,” potentially due to TXN’s role in downregulating the co-stimulatory molecule CD40. These results indicate that TXN expression levels could serve as a predictive biomarker for patient response to ICB, aiding in the identification of individuals who may benefit from such treatments. Furthermore, targeting TXN with inhibitors, particularly in combination with ICB, may offer a novel strategy to enhance immune responses in “cold tumors” and improve the overall efficacy of immunotherapy. This study has several limitations. First, its reliance on a public database and retrospective design limits its prognostic value. Real-world data on NSCLC prognosis are needed to better assess the significance of TXN in immunotherapy. Second, there is a lack of prospective studies involving NSCLC patients receiving immunotherapy. Third, the optimal threshold for TXN expression remains undetermined, with the median TXN mRNA expression used as

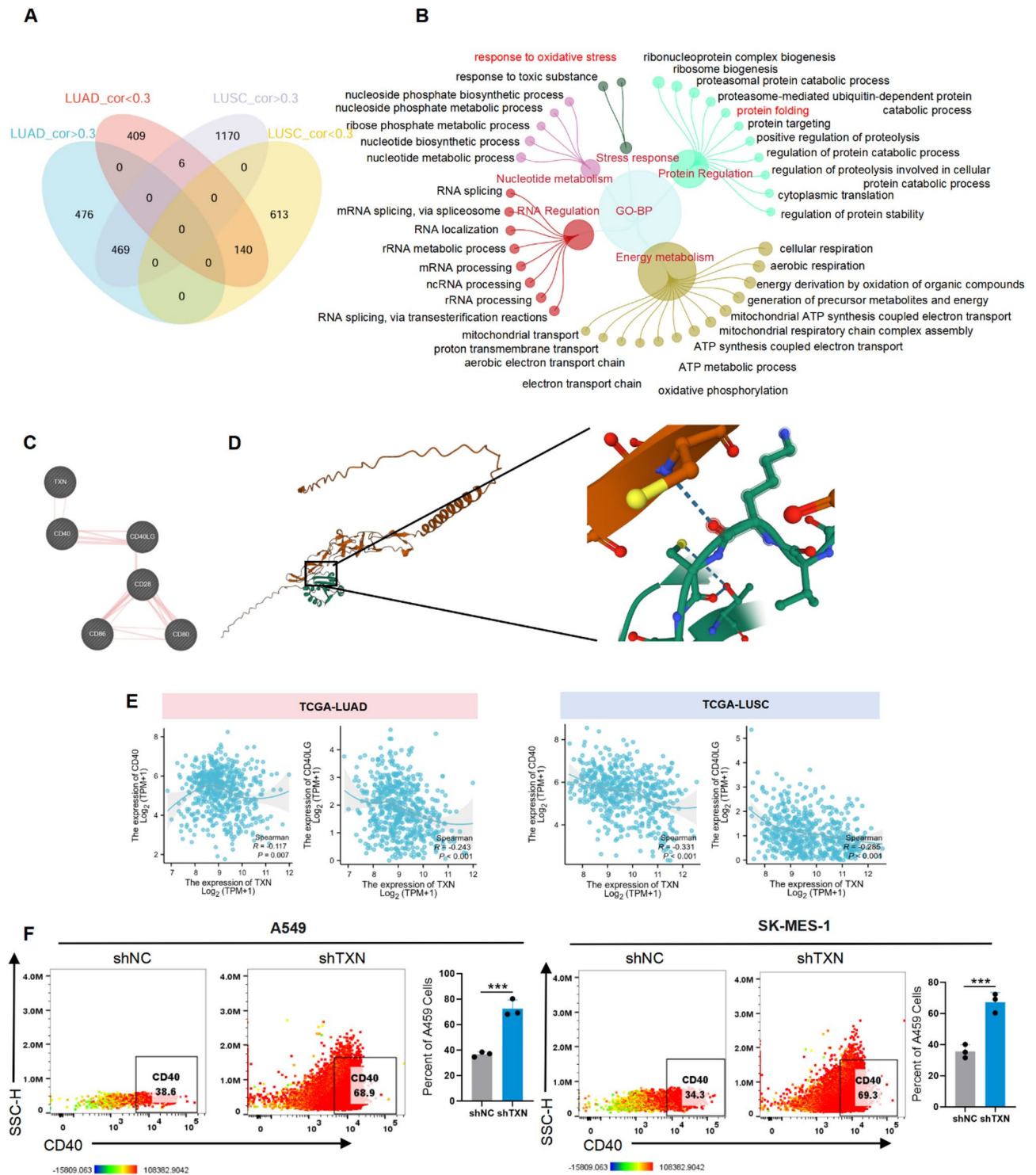


Fig. 5 TXN down-regulates CD40 expression in NSCLC cells. **(A)** Venn diagram of genes positively and negatively correlated with TXN expression in TCGA-LUAD and TCGA-LUSC datasets. **(B)** GO analysis of the intersection of positively and negatively correlated genes in TCGA-LUAD and TCGA-LUSC. **(C)** GeneMANIA network of TXN and CD40 interaction. **(D)** AlphaFold3 predicted TXN and CD40 interaction. **(E)** Correlation between TXN and CD40/CD40L expression in TCGA-LUAD and TCGA-LUSC datasets. **(F)** Flow cytometry analysis of CD40 expression in TXN-stably knocked down A549 and SK-MES-1 cells

a critical value in this study. Finally, further experiments are needed to explore how tumor cell TXN regulates CD40 and suppresses immune responses.

Supplementary Information

The online version contains supplementary material available at <https://doi.org/10.1186/s12931-025-03259-w>.

Supplementary Material 1

Supplementary Material 2

Acknowledgements

This work was supported by the National Natural Science Foundation of China (82002223 to Ji Ping), Natural Science Foundation of Shanghai (24ZR1463300 to Ji Ping), State Key Laboratory of Neurology and Oncology Drug Development (SKLSIM-2024061 to Ji Ping). The results of this study are in part based upon data generated by the TCGA Research Network: <https://www.cancer.gov/tcga>.

Author contributions

P.J. and Y.W. designed the study. Y.W. oversaw the study. J.Y.H. H.Y.W. and A.Y. performed the majority of experiments and analyzed the data. D.Y.Y. and X.W. takes responsibility for the accuracy of the data analysis. P.J. wrote the paper. All authors reviewed the manuscript.

Funding

This work was supported by the National Natural Science Foundation of China (82002223), Natural Science Foundation of Shanghai (24ZR1463300), State Key Laboratory of Neurology and Oncology Drug Development (SKLSIM-2024061).

Data availability

No datasets were generated or analysed during the current study.

Declarations

Ethics approval and consent to participate

This study draws on published research and publicly available data from various consortia. All original studies included in this analysis have been approved by their respective ethical review committees, and informed consent was obtained from all participants. The use of RT-qPCR and WB, in combination with individual-level data, to verify the expression levels of TXN in cancerous and adjacent tissues, was approved by the Ethics Committee of Shanghai Tongji Hospital (ethics approval number: sbtk-2024-246).

Consent for publication

Not applicable.

Competing interests

The authors declare no competing interests.

Clinical trial number

Not applicable.

Received: 24 January 2025 / Accepted: 24 April 2025

Published online: 10 May 2025

References

- Siegel RL, Miller KD, Wagle NS, Jemal A. Cancer statistics, 2023. *CA Cancer J Clin.* 2023;73(1):17–48.
- Sun Q, Hong Z, Zhang C, Wang L, Han Z, Ma D. Immune checkpoint therapy for solid tumours: clinical dilemmas and future trends. *Signal Transduct Target Ther.* 2023;8(1):320.
- Ng KW, Boumelha J, Enfield K, et al. Antibodies against endogenous retroviruses promote lung cancer immunotherapy. *Nature.* 2023;616(7957):563–73.
- Tomita Y, Ikeda T, Sakata S, et al. Association of probiotic *Clostridium butyricum* therapy with survival and response to immune checkpoint blockade in patients with lung cancer. *Cancer Immunol Res.* 2020;8(10):1236–42.
- Reck M, Rodríguez-Abreu D, Robinson AG, et al. Five-Year outcomes with pembrolizumab versus chemotherapy for metastatic Non-Small-Cell lung Cancer with PD-L1 tumor proportion score ≥ 50 . *J Clin Oncol.* 2021;39(21):2339–49.
- Gadgeel SM, Rodríguez-Abreu D, Halmos B, et al. Pembrolizumab plus chemotherapy for metastatic NSCLC with programmed cell death ligand 1 tumor proportion score less than 1%: pooled analysis of outcomes after five years of Follow-Up. *J Thorac Oncol.* 2024;19(8):1228–41.
- Zhang C, Zhang C, Wang H. Immune-checkpoint inhibitor resistance in cancer treatment: current progress and future directions. *Cancer Lett.* 2023;562:216182.
- Lahiri A, Maji A, Potdar PD, et al. Lung cancer immunotherapy: progress, pitfalls, and promises. *Mol Cancer.* 2023;22(1):40.
- Tay C, Tanaka A, Sakaguchi S. Tumor-infiltrating regulatory T cells as targets of cancer immunotherapy. *Cancer Cell.* 2023;41(3):450–65.
- Kang JH, Zappasodi R. Modulating Treg stability to improve cancer immunotherapy. *Trends Cancer.* 2023;9(11):911–27.
- Zheng S, Wang X, Zhao D, Liu H, Hu Y. Calcium homeostasis and cancer: insights from Endoplasmic reticulum-centered organelle communications. *Trends Cell Biol.* 2023;33(4):312–23.
- Chen X, Cubillos-Ruiz JR. Endoplasmic reticulum stress signals in the tumour and its microenvironment. *Nat Rev Cancer.* 2021;21(2):71–88.
- Hetz C, Zhang K, Kaufman RJ. Mechanisms, regulation and functions of the unfolded protein response. *Nat Rev Mol Cell Biol.* 2020;21(8):421–38.
- Hetz C. The unfolded protein response: controlling cell fate decisions under ER stress and beyond. *Nat Rev Mol Cell Biol.* 2012;13(2):89–102.
- Ren J, Bi Y, Sowers JR, Hetz C, Zhang Y. Endoplasmic reticulum stress and unfolded protein response in cardiovascular diseases. *Nat Rev Cardiol.* 2021;18(7):499–521.
- Marciniak SJ, Chambers JE, Ron D. Pharmacological targeting of Endoplasmic reticulum stress in disease. *Nat Rev Drug Discov.* 2022;21(2):115–40.
- Kim YJ, Lee WS, Ip C, Chae HZ, Park EM, Park YM. Prx1 suppresses radiation-induced c-Jun NH2-terminal kinase signaling in lung cancer cells through interaction with the glutathione S-transferase Pi/c-Jun NH2-terminal kinase complex. *Cancer Res.* 2006;66(14):7136–42.
- Egler RA, Fernandes E, Rothermund K, et al. Regulation of reactive oxygen species, DNA damage, and c-Myc function by Peroxiredoxin 1. *Oncogene.* 2005;24(54):8038–50.
- Cao J, Schulte J, Knight A, et al. Prdx1 inhibits tumorigenesis via regulating PTEN/AKT activity. *EMBO J.* 2009;28(10):1505–17.
- Fiskus W, Saba N, Shen M, et al. Auranofin induces lethal oxidative and Endoplasmic reticulum stress and exerts potent preclinical activity against chronic lymphocytic leukemia. *Cancer Res.* 2014;74(9):2520–32.
- Poet GJ, Oka OB, van Lith M, et al. Cytosolic thioredoxin reductase 1 is required for correct disulfide formation in the ER. *EMBO J.* 2017;36(5):693–702.
- Hu J, Zhang L, Xia H, et al. Tumor microenvironment remodeling after neoadjuvant immunotherapy in non-small cell lung cancer revealed by single-cell RNA sequencing. *Genome Med.* 2023;15(1):14.
- Hao Y, Stuart T, Kowalski MH, et al. Dictionary learning for integrative, multimodal and scalable single-cell analysis. *Nat Biotechnol.* 2024;42(2):293–304.
- Hao Y, Hao S, Andersen-Nissen E, et al. Integrated analysis of multimodal single-cell data. *Cell.* 2021;184(13):3573–e358729.
- Stuart T, Butler A, Hoffman P, et al. Comprehensive integration of Single-Cell data. *Cell.* 2019;177(7):1888–e190221.
- Hänzelmann S, Castelo R, Guinney J. GSEA: gene set variation analysis for microarray and RNA-seq data. *BMC Bioinformatics.* 2013;14:7.
- Bischoff P, Trinks A, Obermayer B, et al. Single-cell RNA sequencing reveals distinct tumor microenvironmental patterns in lung adenocarcinoma. *Oncogene.* 2021;40(50):6748–58.
- Jin S, Guerrero-Juarez CF, Zhang L, et al. Inference and analysis of cell-cell communication using cellchat. *Nat Commun.* 2021;12(1):1088.
- Hu C, Li T, Xu Y, et al. CellMarker 2.0: an updated database of manually curated cell markers in human/mouse and web tools based on scRNA-seq data. *Nucleic Acids Res.* 2023;51(D1):D870–6.
- Xu L, Deng C, Pang B, et al. TIP: A web server for resolving tumor immunophenotype profiling. *Cancer Res.* 2018;78(23):6575–80.

31. Chan TA, Yarchoan M, Jaffee E, et al. Development of tumor mutation burden as an immunotherapy biomarker: utility for the oncology clinic. *Ann Oncol*. 2019;30(1):44–56.
32. Karnell JL, Rieder SA, Ettinger R, Kolbeck R. Targeting the CD40-CD40L pathway in autoimmune diseases: humoral immunity and beyond. *Adv Drug Deliv Rev*. 2019;141:92–103.
33. Bullock T. CD40 stimulation as a molecular adjuvant for cancer vaccines and other immunotherapies. *Cell Mol Immunol*. 2022;19(1):14–22.
34. Roselli M, Mineo TC, Basili S, et al. Soluble CD40 ligand plasma levels in lung cancer. *Clin Cancer Res*. 2004;10(2):610–4.
35. Son CH, Lee HR, Koh EK, et al. Combination treatment with decitabine and ionizing radiation enhances tumor cells susceptibility of T cells. *Sci Rep*. 2016;6:32470.
36. Yoshida H, Matsui T, Yamamoto A, Okada T, Mori K. XBP1 mRNA is induced by ATF6 and spliced by IRE1 in response to ER stress to produce a highly active transcription factor. *Cell*. 2001;107(7):881–91.
37. Bertolotti A, Zhang Y, Hendershot LM, Harding HP, Ron D. Dynamic interaction of bip and ER stress transducers in the unfolded-protein response. *Nat Cell Biol*. 2000;2(6):326–32.
38. Senft D, Ronai ZA. UPR, autophagy, and mitochondria crosstalk underlies the ER stress response. *Trends Biochem Sci*. 2015;40(3):141–8.
39. Mimura N, Fulcinitti M, Gorgun G, et al. Blockade of XBP1 splicing by Inhibition of IRE1 α is a promising therapeutic option in multiple myeloma. *Blood*. 2012;119(24):5772–81.
40. Verfaillie T, Garg AD, Agostinis P. Targeting ER stress induced apoptosis and inflammation in cancer. *Cancer Lett*. 2013;332(2):249–64.
41. Andor A, Mohanraj M, Pató ZA, et al. TXNL1 has dual functions as a redox active thioredoxin-like protein as well as an ATP- and redox-independent chaperone. *Redox Biol*. 2023;67:102897.
42. Kar A, Paramasivam B, Jayakumar D, Swaroop AK, Jubie S. Thioredoxin interacting protein inhibitors in diabetes mellitus: A critical review. *Curr Drug Res Rev*. 2023;15(3):228–40.
43. Gencheva R, Arnér E. Thioredoxin reductase Inhibition for Cancer therapy. *Annu Rev Pharmacol Toxicol*. 2022;62:177–96.
44. Prasad CB, Oo A, Liu Y, et al. The thioredoxin system determines CHK1 inhibitor sensitivity via redox-mediated regulation of ribonucleotide reductase activity. *Nat Commun*. 2024;15(1):4667.
45. Fidyk K, Pastorczak A, Goral A, et al. Targeting the thioredoxin system as a novel strategy against B-cell acute lymphoblastic leukemia. *Mol Oncol*. 2019;13(5):1180–95.
46. Sudhadevi T, Harjith A. Thioredoxin: an antioxidant, a therapeutic target and a possible biomarker. *Pediatr Res*. 2024;96(5):1117–9.
47. Bradford HF, McDonnell T, Stewart A, et al. Thioredoxin is a metabolic rheostat controlling regulatory B cells. *Nat Immunol*. 2024;25(5):873–85.
48. McCann K, von Witzleben A, Thomas J, et al. Targeting the tumor mutanome for personalized vaccination in a TMB low non-small cell lung cancer. *J Immunother Cancer*. 2022;10(3):e003821.
49. Zhang J, Wang J, Qian Z, Han Y. CCR5 is associated with immune cell infiltration and prognosis of lung Cancer. *J Thorac Oncol*. 2019;14(5):e1102–3.
50. Cheng Y, Mo F, Li Q, et al. Targeting CXCR2 inhibits the progression of lung cancer and promotes therapeutic effect of cisplatin. *Mol Cancer*. 2021;20(1):62.
51. Kim JY, Kim HJ, Jung CW, Lee TS, Kim EH, Park MJ. CXCR4 uses STAT3-mediated slug expression to maintain radioresistance of non-small cell lung cancer cells: emerges as a potential prognostic biomarker for lung cancer. *Cell Death Dis*. 2021;12(1):48.
52. Liu H, Cheng Q, Xu DS, et al. Overexpression of CXCR7 accelerates tumor growth and metastasis of lung cancer cells. *Respir Res*. 2020;21(1):287.
53. Rosenthal R, Cadieux EL, Salgado R, et al. Neoantigen-directed immune escape in lung cancer evolution. *Nature*. 2019;567(7749):479–85.
54. Lonberg N, Korman AJ. Masterful antibodies: checkpoint Blockade. *Cancer Immunol Res*. 2017;5(4):275–81.
55. Rowshanravan B, Halliday N, Sansom DM. CTLA-4: a moving target in immunotherapy. *Blood*. 2018;131(1):58–67.
56. Qin S, Xu L, Yi M, Yu S, Wu K, Luo S. Novel immune checkpoint targets: moving beyond PD-1 and CTLA-4. *Mol Cancer*. 2019;18(1):155.
57. Danese S, Sans M, Fiocchi C. The CD40/CD40L costimulatory pathway in inflammatory bowel disease. *Gut*. 2004;53(7):1035–43.
58. Battaglia E, Biancone L, Resegotti A, Emanuelli G, Fronda GR, Camussi G. Expression of CD40 and its ligand, CD40L, in intestinal lesions of Crohn's disease. *Am J Gastroenterol*. 1999;94(11):3279–84.
59. Elgueta R, Benson MJ, de Vries VC, Wasiuk A, Guo Y, Noelle RJ. Molecular mechanism and function of CD40/CD40L engagement in the immune system. *Immunol Rev*. 2009;229(1):152–72.
60. database, Liu BEST, Liu Z, Weng L. BEST: a web application for comprehensive biomarker exploration on large-scale data in solid tumors. *J Big Data*. 2023;10:165. <https://doi.org/10.1186/s40537-023-00844-y>.

Publisher's note

Springer Nature remains neutral with regard to jurisdictional claims in published maps and institutional affiliations.